Cyclorotation Models for Eyes and Cameras

Miles Hansard and Radu Horaud

***Abstract*—The human visual system obeys Listing's law, which means that the cyclorotation of the eye (around the line of sight) can be predicted from the direction of the fixation point. It is shown here that Listing's law can conveniently be formulated in terms of rotation matrices. The function that defines the observed cyclorotation is derived in this representation. Two polynomial approximations of the function are developed, and the accuracy of each model is evaluated by numerical integration over a range of gaze directions. The error of the simplest approximation for typical eye movements is less than half a degree. It is shown that, given a set of calibrated images, the effect of Listing's law can be simulated in a way that is physically consistent with the original camera. This condition is important for robotic models of human vision, which typically do not reproduce the mechanics of the oculomotor system.**

***Index Terms*—Biological control systems, robot kinematics, visual system.**

I. Introduction

THIS PAPER uses geometric and numerical methods to explore a kinematic property of human eye-movements. The objective is to model the rotation of the human eye in terms of the standard camera model from computer vision [1]. This paper is motivated by the need to use real image data in computational models of the human vision. It will be shown, in particular, that the images from a standard robotic camera mounting can be made compatible with the observed orientations of the human eye. This result means that subsequent geometric analysis of the images will be consistent with the behavior of the oculomotor system. The results described here provide a foundation for further development of both monocular and binocular models of biological vision [2]–[4].

A. Visual Orientation

There are several types of human eye movements, including those that are used to stabilize the retinal image during motion of the head and those that are specific to binocular vision [5]. This paper, however, is chiefly concerned with *saccadic* eye movements, which are used to fixate visual targets in the scene.

The fixation of a target point defines the *direction* but not the complete *orientation* of the eye, because the orientation includes the "cyclorotation" around the ray that joins the optical center[1] to the target, as well as the direction. In geometric terms, the direction can be specified by a suitable choice of two spherical angles, e.g., elevation and azimuth. The orientation involves a third angle, which accounts for the cyclorotation or "torsion" around the line of sight. Listing's law, as will be explained, describes the observed relationship between visual direction and orientation.

The complete orientation of the eye can consistently be determined from the gaze direction as follows. Suppose that the visual target is represented, with respect to a reference direction, by elevation and azimuth angles α and β. Then, the cyclorotation γ can be treated as a function $\gamma(\alpha, \beta)$. This relation is the principle behind *Donders' law* [5], [6], which states that the actual torsion of the eye is determined by the gaze direction so that the final orientation is fully determined by the visual target. Note, however, that Donders' law does not actually *define* the function $\gamma(\alpha, \beta)$.

B. Ocular Kinematics

Donders' law asserts that torsion is consistently determined by the oculomotor system but does not make any further predictions. A more specific model can be formulated by noting that, given an initial orientation, the subsequent angles and axes of rotation can be used to predict the final torsion.

Hence, the actual cyclorotation function $\gamma(\alpha, \beta)$ can be derived from a geometric model of visual orientation. This fact is the principle behind Listing's law, which quantifies Donders' law as follows: *There exists a unique reference orientation such that any other observed orientation of the eye can be obtained by a single rotation around an axis perpendicular to the reference direction* [5], [6]. It follows that, although the axis of rotation depends on the target direction, it must lie in *Listing's plane*, which is itself perpendicular to the reference direction. The unique reference orientation of the eye is called the *primary position*. The reference direction, which is determined by experiment, is approximately straight ahead. It follows that Listing's plane is approximately parallel to the face [7]. Note that Listing's law does not determine the rotational *movement* of the eye; rather, it states that the observed torsion is compatible with a particular choice of rotation.

Listing's law is applicable if the head is upright and static and if the fixation point is distant. The torsion, in these conditions, can be predicted with an accuracy of around 1° [5], [7]. Listing's law can be extended to describe the case in which the eye moves from a general (i.e., nonprimary) position. The rotation axes remain coplanar in this case, but the plane is

Manuscript received October 22, 2008; revised February 26, 2009. This work was supported in part by the Perception-on-Purpose Project of the European Union under Grant 027268. This paper was recommended by Associate Editor S. Sarkar.

The authors are with the Institut National de Recherche en Informatique et en Automatique (INRIA) Rhône-Alpes, 38330 Montbonnot, France (e-mail: miles.hansard@inrialpes.fr; radu.horaud@inrialpes.fr).

Digital Object Identifier 10.1109/TSMCB.2009.2024211

[1]It will be assumed that the eye has a fixed center of rotation and that this point coincides with the optical center [5].

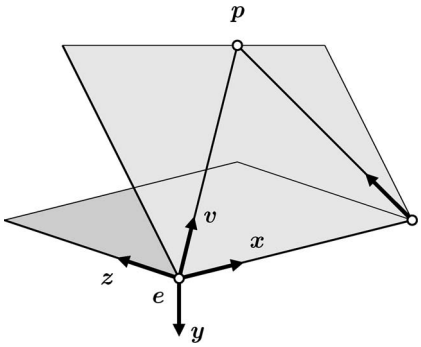

Fig. 1. Two eyes fixate a point $\boldsymbol{p}$ in the scene, which is shown here from the back left. The rotation of one eye (here, the left), with optical center $\boldsymbol{e}$, will be analyzed with respect to the coordinate system $\{\boldsymbol{x}, \boldsymbol{y}, \boldsymbol{z}\}$. The vectors $\boldsymbol{x}$ and $\boldsymbol{z}$ correspond to the interocular and straight-ahead directions, respectively. The vector $\boldsymbol{v}$ corresponds to the visual direction of $\boldsymbol{p}$ from the left optical center $\boldsymbol{e}$. Note that the left and right visual directions lie in a common epipolar plane.

no longer orthogonal to the initial direction [6], [8]. Most of the relevant experimental literature is concerned with primate vision, although support for Listing's law has also been found in other species, including chameleons [9].

Donders' law can be justified with respect to the kinematics of the eye, i.e., cyclorotation is not a component of visual direction, and thus, the oculomotor control problem can be simplified by removing this degree of freedom. Experimental evidence suggests that the human eye is not mechanically constrained to behave this way. For example, irregular torsion is observed in eye movements that occur during sleep [10]. The particular form of Listing's law has been justified with respect to both "motor" and "visual" criteria. For example, it has been shown that the law is related to the minimization of muscular effort, total cyclorotation, and binocular disparity [4], [6], [11].

It is useful, as previously explained, to think of Donders' law as a rule $\gamma(\alpha, \beta)$ that associates a cyclorotation angle γ with each visual direction (α, β) such that the complete orientation of the eye is given by the following three angles: 1) α; 2) β; and 3) $\gamma(\alpha, \beta)$. To derive the form of this function from Listing's law, it is first necessary to define the parameterization of visual direction. Here, the angles α and β will be assigned to the elevation and azimuth of the target, respectively. This pair is the "Helmholtz" coordinate system [4], [6], [12]–[14], in which the visual direction swings in a plane that contains the interocular axis; the plane itself rotates *around* the interocular axis, as shown in Fig. 1.

This azimuth−elevation scheme is the natural choice due to four related reasons. First, it means that torsion can be measured with respect to a reference plane, defined by the two optical centers and the fixation point, which is intrinsic to the viewing configuration. There is no need for an external definition of "horizontal" and "vertical". Second, the elevation of any visual direction can be adjusted without affecting the azimuth. This case is desirable with respect to the measurement of eye movements, because the straight-ahead azimuth is easily defined (by making the visual direction orthogonal to the interocular axis), whereas the straight-ahead elevation is more difficult to determine [5]. Third, the geometry of binocular vision can more readily be described in Helmholtz coordinates, because each elevation plane contains corresponding epipolar lines in the left and right images [15]. Fourth, the definition of $\gamma(\alpha, \beta)$ is simple and symmetric in the Helmholtz coordinate system (see Section VI). The alternative definition in "Fick" coordinates [5], [16], where α and β are the longitude and latitude, respectively, is less concise.

C. Robotic Systems

The Helmholtz scheme is also the natural configuration for an active binocular robot head [17], [18], because the left and right pan motors can be fixed parallel to each other such that the visual axes are coplanar. It follows that, as the cameras converge, the axes will (ideally) intersect in space. Hence, binocular fixation can mechanically be approximated. This type of robot does not obey Listing's law, as will be shown in Section V. However, to simulate the human vision with such a system, the method in Section IX can be used to appropriately cyclorotate the original images. This paper, to simulate human vision, provides an alternative to the mechanical implementation of Listing's law [19], [20]. Robot heads of the latter type are, compared with the Helmholtz configuration, more difficult to construct and control [17].

D. Gaze Tracking

Listing's law is also relevant to the design of gaze-tracking systems [21], [22]. For example, greater accuracy can be achieved by accounting for the small angular difference between the line of sight (defined in relation to the fovea) and the optical axis of the eye [5], [23]. If the latter can be estimated, then the plane that contains the two rays can be obtained from Listing's law. The line of sight is at a fixed angular offset, in this plane, from the optical axis [24]. Listing's law can also be used to relate the direction of gaze to the projection of the iris in a calibrated video of the eye [25].

E. Geometric Models

The mathematical expression of Listing's law depends on the representation of the relevant eye movements. The 3-D rotation group can be parameterized in several different ways [26]. The quaternion [8], [12], [14], rotation vector [27], [28], and geometric algebra [29] parameterizations, which are closely related, are particularly well suited to the modeling of ocular kinematics. It is also possible to represent a rotation by a pair of reflections, which leads to a more geometric interpretation of Listing's law [30]. This paper emphasizes the computational aspects of Listing's law, which is formulated here in terms of rotation matrices. The matrix representation has the advantages of being both mathematically familiar and computationally convenient. Furthermore, it can immediately be combined with standard projection models from the computer vision literature. This result is useful for geometric analysis of the retinal image in relation to Listing's law, as described in Section IX.

F. Novel Contributions

This paper describes new results in the representation, approximation, and simulation of Listing's law. Primarily, a

new derivation of the torsion function $\gamma(\alpha, \beta)$ is made in Sections IV–VI. There are two objectives here. First, Listing's law will be expressed in terms of rotation matrices so that it can readily be incorporated into the standard camera model of computer vision [1]. Second, these rotation matrices will be suitable for the analysis of binocular vision. This objective means that the results that were obtained here provide a foundation for further analysis of binocular kinematics [2].

Two approximations (one of which has previously been used, e.g., [4]) of the Listing cyclorotation are made in Section VII. The advantage of these approximations is that they dispense with the trigonometric functions in the exact formula, which makes it easier to incorporate cyclorotation into theoretical models of oculomotor control [3], [4]. The aforementioned results are visualized by stereographic projection. The objective of the visualization is to understand the pattern of cyclorotation across the visual field.

A procedure for the numerical integration of ocular torsion is introduced in Section VIII, where it is used to estimate the accuracy of the aforementioned approximate cyclorotation models. This numerical evaluation is complementary to the analytic approach that has been taken elsewhere [11]. The objective is to establish the range of visual directions over which the approximate models can be used. This evaluation also justifies the approximations that have been used in previous work (e.g., [3] and [4]).

Finally, in Section IX, an algorithm for the simulation of Listing's law is presented. The proper way of simulating ocular torsion, given a set of calibrated images, has previously not been addressed. Here, the objective is to understand how cyclorotation relates to the extrinsic and intrinsic parameters of the camera [1].

G. Organization of the Paper

This paper is organized as follows. Section II introduces the necessary notation and defines the primary position of the eye. A useful visualization procedure based on stereographic projection is described in Section III. Matrix representations of Listing and Helmholtz orientation are developed in Sections IV and V, respectively. The Listing cyclorotation is derived in Section VI. Approximations of the cyclorotation are developed in Section VII. The accuracy of each approximation is evaluated in Section VIII. It is shown in Section IX that, given a set of images, the preceding results can be used to simulate the effects of ocular torsion. Section X contains the conclusion of this paper.

II. Scene Coordinates

Each scene point $\boldsymbol{p} = (x, y, z)^\top$ is represented in a head-fixed coordinate system, as illustrated in Fig. 1. The origin is located at the rotational center of the left eye, $\boldsymbol{e} = (0, 0, 0)^\top$, which is assumed to coincide with the optical center [5]. The axes of the coordinate system are $\{\boldsymbol{x}, \boldsymbol{y}, \boldsymbol{z}\}$, with $\boldsymbol{x}$ and $\boldsymbol{y}$ being parallel to the coronal ("face") plane. The vector $\boldsymbol{x}$ points rightward along the interocular axis (according to the subject's point of view), whereas $\boldsymbol{y}$ points downward. The coordinate system is right handed, and thus, it follows that $\boldsymbol{z}$ is perpendicular to the coronal plane and points out into the scene. It will be assumed that, when the eye is in the primary position, $\boldsymbol{z}$ is aligned with the visual axis. The plane that is perpendicular to $\boldsymbol{x}$ intersects the eyeball in a great circle, which, in the primary position, defines the *vertical meridian* of the eye. The plane that is perpendicular to the $\boldsymbol{y}$ axis defines, in the primary position, the *horizontal meridian* of the eye. It will be assumed that these meridians are fixed on the eye (not in the head).

The target point is $\boldsymbol{p}$, which lies in a visual direction represented by the unit vector

$$\boldsymbol{v} = \boldsymbol{p}/d \tag{1}$$

where $d = |\boldsymbol{p}|$ is the Euclidean distance to $\boldsymbol{p}$. The target point is fixated by a rotation of the primary line of sight $\boldsymbol{z}$ onto the target direction $\boldsymbol{v}$. This instance will be expressed as

$$\boldsymbol{R}\boldsymbol{z} = \boldsymbol{v} \tag{2}$$

where $\boldsymbol{R}$ is a 3×3 rotation matrix. If the target point lies in either the horizontal plane $\{\boldsymbol{x}, \boldsymbol{z}\}$ or the vertical plane $\{\boldsymbol{y}, \boldsymbol{z}\}$, then the eye is in the *secondary position* after the rotation. The fixation of a generic scene point leaves the eye in the *tertiary* position [5].

It will be assumed, in the following sections, that the eye begins in the primary position $\boldsymbol{z}$ and rotates to fixate the target point $\boldsymbol{p}$. If the eye begins in a nonprimary position, then it can be shown that Listing's plane is rotated in space by half the angle of the initial direction [7], [30]. This case will not be analyzed here.

Several different coordinate conventions have been used in the literature (e.g., [6], [8], and [12]). The aforementioned system was chosen for two reasons. First, it is consistent with the computer vision literature, in which $\boldsymbol{z}$ is usually the optical axis. Second, it is convenient in the binocular case, which emphasizes the family of planes that contain the interocular axis. Here, the convention of $\boldsymbol{x}$ that points rightward is kept for these planes.

III. Stereographic Projection

The orientation of the eye is visualized in this paper by stereographic projection [5], [6]. This procedure, which is illustrated in Fig. 2, is defined as follows. The eyeball is represented by the unit sphere $\mathcal{S}$ located at $\boldsymbol{e}$. The stereographic center of projection $\boldsymbol{s}_0 = (0, 0, -1)^\top$ is fixed in the head, at the back of the eye-socket. A projection plane $\mathcal{T}$ is fixed in space perpendicular to the $\boldsymbol{z}$-axis. Now, consider a landmark on the eyeball, with coordinates $(v_x, v_y, v_z)^\top$; this point, together with $\boldsymbol{s}_0$, defines a ray. The intersection of the ray with the plane $\mathcal{T}$ defines the stereographic projection (ξ, η) of the landmark. For example, if $\mathcal{T}$ passes through the center of $\mathcal{S}$, then the projection is

$$(\xi, \eta) = \frac{(v_x, v_y)}{1 + v_z}. \tag{3}$$

Any point other than $\boldsymbol{s}_0$ can be mapped to the plane this way. In particular, the entire forward hemisphere of visual

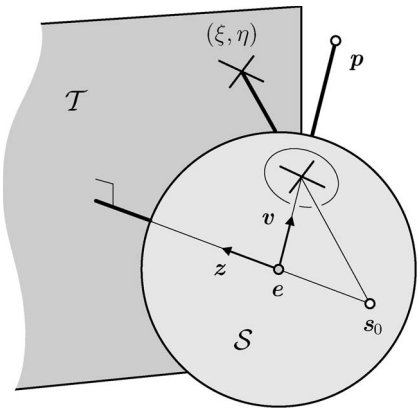

Fig. 2. Stereographic projection. A schematic of the procedure for constructing Figs. 4, 5, 7, and 8. The eyeball, which is centered at the point $\boldsymbol{e}$, is shown from the back left, as shown in Fig. 1. The stereographic plane $\mathcal{T}$ is perpendicular to the head-fixed $\boldsymbol{z}$-axis. The eye fixates a scene point $\boldsymbol{p}$; the corresponding vector $\boldsymbol{v}$ points *into* the page. A reference cross, which is fixed to the cornea, is projected onto $\mathcal{T}$. The center of projection $\boldsymbol{s}_0$ is fixed in the head, at the back of the eye.

directions $\{\boldsymbol{v} : |\boldsymbol{v}| = 1, v_z \geq 0\}$ is mapped to the unit disc, which is centered at $(0, 0)^\top$ in $\mathcal{T}$.

The orientation of the eye will be visualized by projecting a notional cross, which is marked on the cornea of the eye and aligned with the pair planes that contain the horizontal and vertical retinal meridians. If the eye rotates to fixate a point $\boldsymbol{p}$, then the cross will take coordinates $(v_x, v_y, v_z)^\top$, which can be projected to (ξ, η) by (3). The procedure is illustrated in Fig. 2, where, for clarity, the plane $\mathcal{T}$ is shown *in front* of the eyeball (the principle is the same).

The stereographic projection preserves several properties of the underlying rotation group [26]. This case means that the procedure gives an effective visualization of ocular orientation, as shown in Figs. 4 and 5. For example, consider the "spokes" of parallel crosses that appear in Fig. 5(a); these spokes correspond to *geodesic paths* through the space of orientation. The eye directly moves from the central point, with no additional rotation of the cross.

It should be emphasized that, in this paper, stereographic projection is used only for visualization. It is *not* used to describe the retinal projection of the scene. Indeed, the stereographic and optical centers of projection, $\boldsymbol{s}_0$ and $\boldsymbol{e}$, respectively, are quite distinct (see Fig. 2).

IV. Listing Orientation

Listing's law states that the actual orientation of the eye, while $\boldsymbol{p}$ is fixated, is consistent with a rotation of the primary line of sight $\boldsymbol{z} = (0, 0, 1)^\top$ around a perpendicular axis $\boldsymbol{w}$. It follows that, for any target $\boldsymbol{p}$, the corresponding axis $\boldsymbol{w}$ is in the plane $\{\boldsymbol{x}, \boldsymbol{y}\}$, which, in this context, is Listing's plane. The axis is defined as

$$\boldsymbol{w} = \boldsymbol{z} \times \boldsymbol{v} \tag{4}$$

$$= \sin(\phi)(\sin\theta, \cos\theta, 0)^\top \tag{5}$$

where ϕ is the angle of rotation (from $\boldsymbol{z}$ to $\boldsymbol{v}$), and θ is the direction of the axis in the $\{\boldsymbol{x}, \boldsymbol{y}\}$ plane, as shown in Fig. 3. The

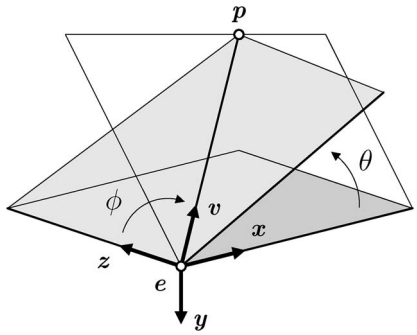

Fig. 3. Listing coordinates (see Fig. 6). The optical center of the eye is located at point $\boldsymbol{e} = (0, 0, 0)^\top$. The initial gaze direction, with the eye being in the "primary position," is along the $\boldsymbol{z}$-axis. To fixate the point $\boldsymbol{p}$, a rotation through angle ϕ is required. The axis $\boldsymbol{w}$ of the rotation is *perpendicular* to the $\{\boldsymbol{z}, \boldsymbol{v}\}$ plane and *in* the $\{\boldsymbol{x}, \boldsymbol{y}\}$ plane. The axis is inclined from the vertical by an angle θ.

angle θ is in the range $0 \leq \theta < 2\pi$; in particular, if $\theta = 0$, then $\boldsymbol{w}$ is parallel to $\boldsymbol{y}$, and the rotated line of sight lies in the $\{\boldsymbol{x}, \boldsymbol{z}\}$ plane. The angle ϕ can unambiguously be recovered from

$$\sin\phi = \sqrt{\boldsymbol{w} \cdot \boldsymbol{w}} \tag{6}$$

because of the physical constraint $0 \leq \phi \leq \pi/2$.

The axis $\boldsymbol{w}$ and angle ϕ define the Listing rotation, which will be represented by a 3×3 matrix $\boldsymbol{R}_L$. Rodrigues' equation [26] is used to compute $\boldsymbol{R}_L$ from $\boldsymbol{w}$ and ϕ, which results in

$$\begin{aligned} \boldsymbol{R}_L &= (\boldsymbol{X}_L, \boldsymbol{y}_L, \boldsymbol{z}_L) \\ &= \begin{pmatrix} 1 - \lambda\cos^2\theta & \lambda\cos\theta\sin\theta & \cos\theta\sin\phi \\ \lambda\cos\theta\sin\theta & 1 - \lambda\sin^2\theta & -\sin\theta\sin\phi \\ -\cos\theta\sin\phi & \sin\theta\sin\phi & \cos\phi \end{pmatrix} \end{aligned} \tag{7}$$

where $\boldsymbol{x}_L$, $\boldsymbol{y}_L$ and $\boldsymbol{z}_L$ are the columns of the matrix, and the versine

$$\lambda = 1 - \boldsymbol{z} \cdot \boldsymbol{v} \tag{8}$$

$$= 1 - \cos\phi \tag{9}$$

has been introduced for notational convenience. The vector $\boldsymbol{z}_L$ is the rotated line of sight $\boldsymbol{R}_L\boldsymbol{z}$, whereas $\{\boldsymbol{x}_L, \boldsymbol{y}_L\}$ are the rotated retinal axes. Equation (7) is a mathematical expression of Listing's law (see Section I-B).

The stereographic coordinates of the Listing rotation are shown in Fig. 4(a), where the concentric circles are parameterized by θ, and the radial spokes are parameterized by ϕ. The ocular orientations that result from Listing's law are illustrated in Fig. 5(a). Note that the crosses, each of which encodes the ocular torsion, are parallel in this representation.

V. Helmholtz Orientation

It was shown in the preceding section that the target visual direction $\boldsymbol{v}$ can be reached by a rotation $\boldsymbol{R}_L$ of $\boldsymbol{z}$ around a variable axis $\boldsymbol{w}$. To quantify the torsion that is associated with this rotation, it will be necessary to establish a reference system of rotations. These rotations will be defined with respect to

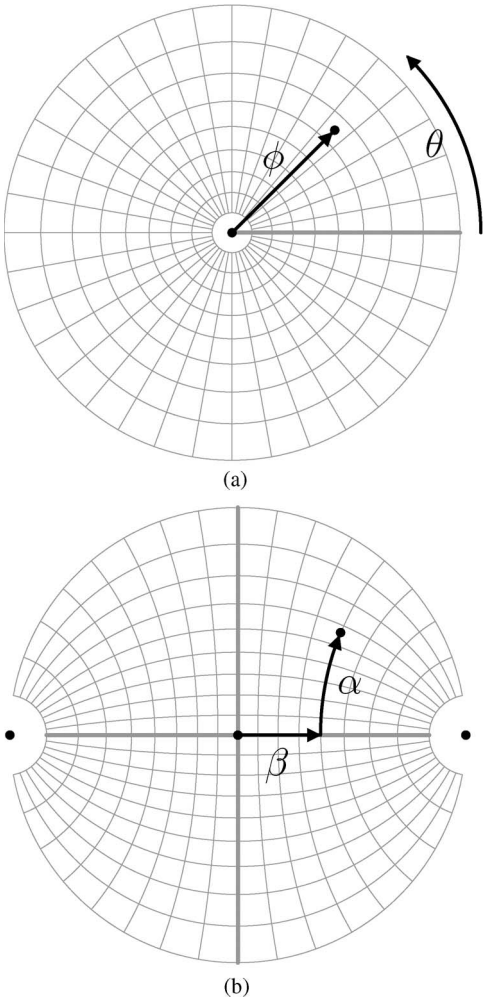

Fig. 4. Stereographic projection of the Listing and Helmholtz coordinate systems. The track from the origin shows the path of the visual axis as the eye turns to fixate in the direction $\theta = 45°$, $\phi = 65°$. Note that this approach involves one rotation in (a) and two rotations in (b). A spacing of $10°$ is used for each family of coordinate lines. (a) Stereographic projection of the Listing coordinate system (θ, ϕ) (see Fig. 3). The primary direction is mapped to the center of the disc; the boundary represents targets at $\phi = 90°$ eccentricity. (b) Stereographic projection of the Helmholtz coordinate system (α, β) (see Fig. 6). The points on the far left and right represent the intersection of the interocular axis with the eyeball.

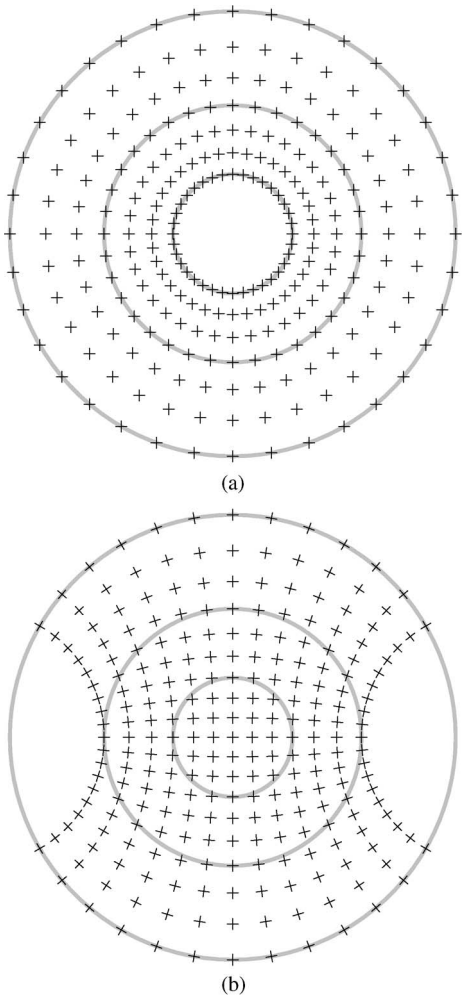

Fig. 5. (a) Stereographic projection of Listing orientations, which are plotted in polar coordinates (θ, ϕ). Note that the retinal orientations are mutually parallel in this representation. Solid circles indicate eccentricities of $30°$, $60°$, and $90°$. Some crosses are omitted in the central region for clarity. (b) Helmholtz orientations, which are plotted in (α, β) coordinates. Note that the retinal orientations are *not* mutually parallel in this representation. The horizontal meridian of each possible orientation lies in an azimuthal plane.

the fixed axes $\{\boldsymbol{x}, \boldsymbol{y}, \boldsymbol{z}\}$. It is, as described in the Introduction, convenient to use the *Helmholtz* rotation, i.e.,

$$\boldsymbol{R}_H = \boldsymbol{A}\boldsymbol{B} \tag{10}$$

where $\boldsymbol{A}$ represents a rotation around $\boldsymbol{x}$, and $\boldsymbol{B}$ represents a rotation around $\boldsymbol{y}$. The two factors are defined as follows. The rotation matrix

$$\boldsymbol{A} = \begin{pmatrix} 1 & 0 & 0 \\ 0 & \cos\alpha & -\sin\alpha \\ 0 & \sin\alpha & \cos\alpha \end{pmatrix} \tag{11}$$

is associated with the *elevation* angle α of the target, and the rotation matrix

$$\boldsymbol{B} = \begin{pmatrix} \cos\beta & 0 & \sin\beta \\ 0 & 1 & 0 \\ -\sin\beta & 0 & \cos\beta \end{pmatrix} \tag{12}$$

is associated with the *azimuth* angle β of the target. The azimuth and the elevation are defined as

$$\tan\alpha = -v_y/v_z \tag{13}$$
$$\sin\beta = v_x/d \tag{14}$$

where d is the distance to the target, as expressed in (1). Note that points with positive elevation are above the optical center $(y < 0)$, whereas points with positive azimuth are at the right of the optical center $(x > 0)$. The angular ranges are $-\pi/2 \leq \alpha \leq \pi/2$ and $-\pi/2 \leq \beta \leq \pi/2$. The Helmholtz rotation is illustrated in Fig. 6.

The explicit form of the Helmholtz matrix $\boldsymbol{R}_H$ is obtained by substituting (11) and (12) into (10) and performing the multiplication, which results in

$$\begin{aligned} \boldsymbol{R}_H &= (\boldsymbol{x}_H, \boldsymbol{y}_H, \boldsymbol{z}_H) \\ &= \begin{pmatrix} \cos\beta & 0 & \sin\beta \\ \sin\alpha\,\sin\beta & \cos\alpha & -\sin\alpha\,\cos\beta \\ -\cos\alpha\,\sin\beta & \sin\alpha & \cos\alpha\,\cos\beta \end{pmatrix}. \end{aligned} \tag{15}$$

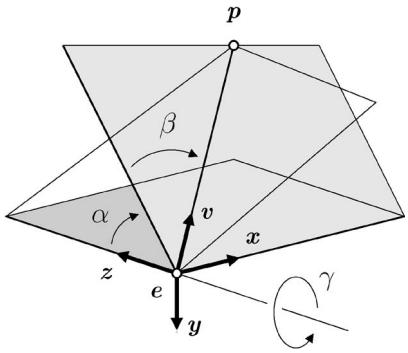

Fig. 6. Helmholtz coordinates (see Fig. 3). The eye turns from the initial direction $\boldsymbol{z}$ to fixate the point $\boldsymbol{p}$, as shown in Fig. 3. This motion is represented as follows. The eye rotates through angle β around the axis $\boldsymbol{y}$, after which the $\{\boldsymbol{x}, \boldsymbol{z}\}$ plane is rotated by angle α around axis $\boldsymbol{x}$. To match the final Listing orientation, an initial cyclorotation around $\boldsymbol{z}$ of angle γ would be required.

Note that, by analogy with (7), $\boldsymbol{z}_H$ is the rotated line of sight $\boldsymbol{R}_H\boldsymbol{z}$, whereas $\{\boldsymbol{x}_H, \boldsymbol{y}_H\}$ are the rotated retinal axes.

The stereographic coordinates of the Helmholtz rotation are shown in Fig. 4(b), where the bottom-to-top curves are parameterized by α, and the left-to-right curves are parameterized by β. Furthermore, note that each left to right curve can be identified with the intersection of an epipolar plane with the viewing sphere. The orientations that result from the Helmholtz rotation scheme are illustrated in Fig. 5(b). It is important to see that the crosses, compared with Fig. 5(a), are no longer parallel. Rather, the "horizontal" axis of each cross lies in the corresponding epipolar plane.

VI. Ocular Torsion

It has been shown in Sections IV and V that the eye can be directed to a target $\boldsymbol{p}$ by a Listing rotation $\boldsymbol{R}_L$ or by a Helmholtz rotation $\boldsymbol{R}_H$; hence

$$\boldsymbol{z}_L = \boldsymbol{z}_H = (v_x, v_y, v_z)^\top \tag{16}$$

where $\boldsymbol{v}$ is the visual direction of $\boldsymbol{p}$, as expressed in (1). The Listing rotation accounts for the observed *orientation* of the eye and for the direction. Hence, if Listing's law is obeyed, then the vectors $\boldsymbol{x}_L$ and $\boldsymbol{y}_L$ are aligned with the horizontal and vertical meridians of the retina. However, the corresponding Helmholtz axes $\boldsymbol{x}_H$ and $\boldsymbol{y}_H$ are, in general, cyclorotated around the common direction $\boldsymbol{v}$.

The discrepancy can be resolved by introducing a third rotation matrix, which represents the torsion around the primary direction $\boldsymbol{z}$. We have

$$\boldsymbol{C} = \begin{pmatrix} \cos\gamma & \sin\gamma & 0 \\ -\sin\gamma & \cos\gamma & 0 \\ 0 & 0 & 1 \end{pmatrix}. \tag{17}$$

Note that this cyclorotation is *counterclockwise* from the subject's point of view (i.e., looking out along the increasing $\boldsymbol{z}$ axis). For example, if $\gamma = \pi/2$, then $\boldsymbol{C}\boldsymbol{y} = \boldsymbol{x}$. This condition is consistent with the sense of θ, which is shown by comparing Figs. 3 and 6.

The Listing rotation $\boldsymbol{R}_L$ can now be represented in the Helmholtz system. The appropriate composition of (10) and (17) gives the equation

$$\boldsymbol{R}_L = \boldsymbol{A}\boldsymbol{B}\boldsymbol{C}. \tag{18}$$

The torsion angle γ in (17), which solves (18), must now be obtained in terms of the Euler angles α and β in (11) and (12). This derivation will be made in two steps. First, the Listing meridian $\boldsymbol{y}_L$ will be expressed in terms of α and β. Second, the inclination of this meridian will be computed in the Helmholtz axes $\boldsymbol{x}_H$ and $\boldsymbol{y}_H$.

It is straightforward to express $\boldsymbol{y}_L$ in terms of the components of $\boldsymbol{z}_L$ by inspection of the second and third columns of the rotation matrix (7). The result, which is written in the notation of (16), is

$$\boldsymbol{y}_L = \left(\frac{-v_x v_y}{1+v_z}, \frac{1+v_z-v_y^2}{1+v_z}, -v_y \right)^\top \tag{19}$$

where the fact that $\sin^2\phi = 1 - \cos^2\phi = (1+v_z)(1-v_z)$ has been used. Equation (19) is the crux of the derivation, because, using the equality (16), the components of $\boldsymbol{v}$ can be substituted from $\boldsymbol{z}_H$, which is defined in the *other* coordinate system (15). Now that both $\boldsymbol{y}_L$ and $\boldsymbol{y}_H$ are known in terms of (α, β), the cosine of the torsion angle is easily obtained as follows:

$$\begin{aligned} \cos\gamma &= \boldsymbol{y}_L \cdot \boldsymbol{y}_H \\ &= \frac{\cos\alpha + \cos^2\alpha\cos\beta + \sin^2\alpha\cos\beta}{1+v_z} \\ &= \frac{\cos\alpha + \cos\beta}{1+\cos\alpha\cos\beta} \end{aligned} \tag{20}$$

where the identity $\cos^2\alpha + \sin^2\alpha = 1$ has been used. This result is sufficient to define the torsion angle as $|\gamma| < \pi/2$. However, it is also possible to compute the sine of the angle as the dot product of $\boldsymbol{y}_L$ with the reference axis $\boldsymbol{x}_H$. By a derivation analogous to (20), we have

$$\begin{aligned} \sin\gamma &= \boldsymbol{y}_L \cdot \boldsymbol{x}_H \\ &= \frac{\sin\alpha\sin\beta}{1+\cos\alpha\cos\beta}. \end{aligned} \tag{21}$$

The cosine and sine equations (20) and (21) can be combined to give the final result, i.e.,

$$\tan\gamma = \frac{\sin\alpha\sin\beta}{\cos\alpha+\cos\beta}. \tag{22}$$

This equation can be put into a useful half-angle form through the trigonometric identity $\tan(\mu/2) = \tan\mu\sin\mu/(\tan\mu + \sin\mu)$. With reference to (21) and (22), this relation gives

$$\tan\frac{\gamma}{2} = \tan\frac{\alpha}{2}\tan\frac{\beta}{2}. \tag{23}$$

The results (22) and (23) were originally obtained by Helmholtz [6], although the current derivation is different.

The meaning of the torsion formula (22) is illustrated in Fig. 7(a). Here, the location of each cross is determined by

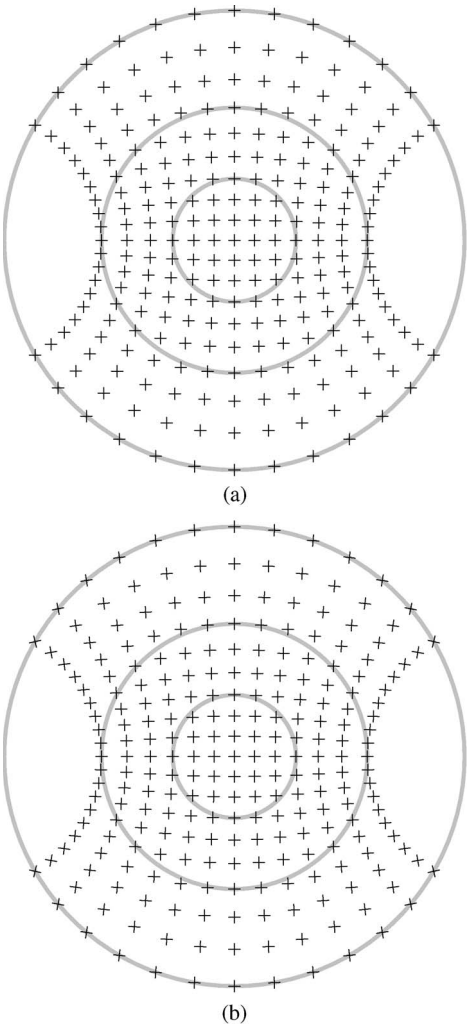

Fig. 7. (a) Listing orientations, which are plotted in $(\alpha\beta)$ coordinates. Each orientation has been subject to a cyclorotation $\gamma(\alpha, \beta)$, which results in mutually parallel stereographic crosses, as shown in Fig. 5. (b) The *approximate* cyclorotation $\gamma_2(\alpha, \beta)$, as defined in equation (25), has been used. The approximation is good for eccentricities of less than 60° (i.e., inside the second gray circle), but some tilting of the crosses is shown in the periphery. See Fig. 8 for a visualization of the difference between (a) and (b).

(α, β), as shown in Fig. 5(b). However, in each direction (α, β), the eye has been cyclorotated by $\gamma(\alpha, \beta)$ in accordance with (22). The result is that the projected crosses are made mutually parallel, as shown in the Listing orientation in Fig. 5(a). Hence, it is shown that Listing's law has been *simulated* in the Helmholtz coordinate system.

Equation (23) shows that the torsion γ will be zero if either α or β is zero. These "secondary positions" of the eye correspond to the parallel crosses on the horizontal and vertical meridians in Fig. 5(b). If α and β are both nonzero, then there are two qualitative cases. If α and β have the same sign, then γ is positive, and the resulting cyclorotation is *counterclockwise* from the subject's point of view [see (17)]. These rotations map each cross in the upper right and lower left quadrants in Fig. 5(b) onto the corresponding cross in Fig. 7(a). If α and β have different signs, then γ is negative, and the rotation is *clockwise*. These rotations map each cross in the upper left and lower right quadrants in Fig. 5(b) onto the corresponding cross in Fig. 7(a).

Consider, for example, the fixation of a distant scene point in the upper midsagittal plane (i.e., "ahead" and "up"), as shown in Fig. 1. This fixation means that the elevation is $\alpha > 0$, whereas the left and right azimuths are $\beta_\ell > 0$ and $\beta_r < 0$, respectively. Then, it follows from (23) that, for each eye that obeys Listing's law, the *nasal* half of the horizontal retinal meridian will turn *up* out of the Helmholtz elevation plane (for example, see [31] and [32]). Furthermore, a rotation [see (17)] of the elevation plane by $\gamma_\ell > 0$ around the left visual axis would align it with the horizontal meridian of the left retina. Likewise, a rotation [see (17)] of the elevation plane by $\gamma_r < 0$ around the right visual axis would align it with the horizontal meridian of the right retina.[2]

The preceding example of "ahead" and "up" fixation can also be described in relation to the *vertical* retinal meridians. In this case, the upper halves of these meridians turn inward (nasally) with respect to the head-fixed vertical direction.[3] This instance is commonly referred to as "intorsion" of the vertical meridians [5].

Note that (18) expresses the Listing rotation $\boldsymbol{R}_L = \boldsymbol{ABC}$ in relation to head-fixed axes $\boldsymbol{x}$, $\boldsymbol{y}$, and $\boldsymbol{z}$. It is straightforward to transform this expression to an eye-fixed representation, i.e., $\boldsymbol{R}_L = \boldsymbol{C}'\boldsymbol{B}'\boldsymbol{A}'$. The matrices $\boldsymbol{C}'$, $\boldsymbol{B}'$ and $\boldsymbol{A}'$ can be obtained from Rodrigues' formula, with axes $\boldsymbol{B}'\boldsymbol{A}'\boldsymbol{z}$, $\boldsymbol{A}'\boldsymbol{y}$, and $\boldsymbol{x}$, respectively.

VII. Approximate Models

The Helmholtz torsion equation (22) is valid over the hemisphere of gaze angles $\alpha, \beta \in [-90°, 90°]$. The maximum range of human eye movements is smaller than this value, and the typical range is much smaller; an average saccade magnitude of 15° has been reported [33]. This result suggests that a simplified form of the torsion function (22) may be valid in practice. Moreover, there are three particular reasons for considering approximate torsion functions: 1) a better understanding of the exact torsion function can be obtained; 2) the ease with which the visual system could represent the function $\gamma(\alpha, \beta)$ is established; and 3) the approximations can be used to simplify the kinematics of the oculomotor system [3], [4].

The Helmholtz torsion function (22), as noted in Section VI, can be expressed in the half-angle form (23), with $\tan(\gamma/2)$ on the left-hand side. Recall the truncated Taylor series $\tan(\sigma) = \sigma + \sigma^3/3 + O(\sigma^5)$. The half-angle version of this series is therefore

$$\tan\frac{\sigma}{2} = \frac{\sigma}{2} + \frac{\sigma^3}{3 \times 2^3} + O(\sigma^5).$$

The corresponding series for $\tan(\alpha/2)$ and $\tan(\beta/2)$ are combined according to (23). The following half-angle approximation is obtained, with discarded terms of total degree 6 (i.e., $3+3$, $1+5$, and $5+1$) and higher:

$$\tan\frac{\gamma}{2} \approx \frac{\alpha\beta}{4} + \frac{\alpha^3\beta}{48} + \frac{\alpha\beta^3}{48}. \tag{24}$$

[2]For comparison with the literature, these are the "*Upper-nasal; Out*" cases in Westheimer's [12, Tables 1 and 2].

[3]Westheimer's "*Upper-nasal; In*" cases [12].

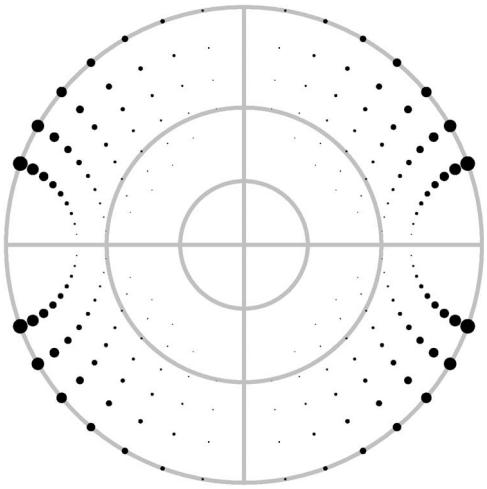

Fig. 8. Visualization of the difference between the actual torsion [see Fig. 7(a)] and the γ_2 approximation [see Fig. 7(b)], as plotted in the $(\alpha\beta)$ coordinates. Larger discs represent worse approximations, as can be confirmed by comparing Fig. 7(a) and (b). Note that the large errors occur in directions with high absolute elevation $|\alpha|$ and high absolute azimuth $|\beta|$. Errors of less than 0.5° are not shown; otherwise, the disc radii are proportional to $|\gamma_2(\alpha,\beta) - \gamma(\alpha,\beta)|$. The horizontal and vertical meridians shown are in gray for reference.

Note that the terms of total degrees 3 and 5 are not in the expansion in (23) due to the saddle-like symmetries of the function.

The inverse tangent can be approximated by the formula $\tan^{-1}(\sigma\tau) = \sigma\tau + O(\sigma^3\tau^3)$, where the total truncation degree matches that of (23). It follows that the second- and fourth-degree approximations of $\gamma(\alpha,\beta)$ are

$$\gamma_2(\alpha,\beta) = \frac{\alpha\beta}{2} \tag{25}$$

$$\gamma_4(\alpha,\beta) = \frac{\alpha\beta}{2} + \frac{\alpha^3\beta}{24} + \frac{\alpha\beta^3}{24}. \tag{26}$$

The first of these approximations [see (25)] has appeared elsewhere (e.g., [4]). It is shown that the approximations are much simpler than the original function [see (22)]; in particular, neither trigonometric nor inverse-trigonometric functions are involved.

The accuracy of the second-degree approximation [see (25)] is visualized in Fig. 7(b). If the approximation were perfect, then this plot would be identical to that in Fig. 7(a). It is shown that, inside the second (60°) circle, the two plots are visually indistinguishable. Differences in cyclorotation can, however, clearly be seen along the outer (90°) circle. The corresponding plot of the fourth-order [see (26)] approximation is visually identical to that in Fig. 7(a). The discrepancy between Fig. 7(a) and (b) is visualized in Fig. 8. A more formal evaluation will be made in the following section.

VIII. Numerical Evaluation

The exact and approximate torsion functions will now be compared over a range of visual directions. This comparison will intuitively be done by moving the eye from the primary position to a new direction and evaluating the resulting torsion. This measurement will be averaged over a continuous range of visual directions. The range of directions will be defined by putting an upper limit on the eccentricity r of a visual target. Hence, it is natural to choose a set of Listing directions, with $0 \le \phi \le r$, which can be converted to Helmholtz coordinates and will be used in (25) and (26). The conversion is obtained by comparing the third columns of the matrices (7) and (15). If, as before, the eccentricity of the target is in the range $0 \le \phi \le \pi/2$, then

$$\alpha(\theta,\phi) = \tan^{-1}\frac{\sin\theta\sin\phi}{\cos\phi} \tag{27}$$

$$\beta(\theta,\phi) = \sin^{-1}(\cos\theta\sin\phi). \tag{28}$$

It is now straightforward to define a function $\delta(\theta,\phi)$, which is the torsion value γ and measured in direction (θ,ϕ) as follows:

$$\delta(\theta,\phi) = \gamma\left(\alpha(\theta,\phi),\beta(\theta,\phi)\right). \tag{29}$$

The functions $\delta_2(\theta,\phi)$ and $\delta_4(\theta,\phi)$ are similarly defined from the approximations γ_2 and γ_4, respectively, [see (25) and (26)]. The torsion error $\epsilon_k(\theta,\phi)$ will also be defined in the Listing coordinates. This function measures the difference between the approximate and actual values, i.e., δ_k and δ, respectively. We have

$$\epsilon_k(\theta,\phi) = \delta_k(\theta,\phi) - \delta(\theta,\phi). \tag{30}$$

The accuracy of the kth-order approximation can be evaluated by integrating a suitable function of ϵ_k over a region of visual directions (θ,ϕ). Such integrals can be studied analytically, but a numerical approach will be preferred here. This choice allows the integrand and the region of integration to be chosen with more freedom. In particular, the absolute value of the error can be integrated.

The notation $|g|_0^r$ represents the functional that returns the average absolute value of a function $g(\theta,\phi)$, which is computed over a range of visual directions $0 \le \theta \le 2\pi$ and $0 \le \phi \le r$. This notation is defined as

$$|g|_0^r = \frac{1}{A(r)}\int_0^{2\pi}\int_0^{r} \sin(\phi)\,|g(\theta,\phi)|\,\mathrm{d}\phi\,\mathrm{d}\theta \tag{31}$$

where $\sin(\phi)$ is the scalar Jacobian. The normalization term $A(r)$ is the area of the spherical cap, over which the integration is performed. This term is easily obtained from the formula

$$A(r) = 2\pi(1-\cos r). \tag{32}$$

The integral (31) was evaluated by a standard numerical routine [34]. Table I shows the results of the evaluation. Each functional $|g|_0^r$ was evaluated for all eye movements up to eccentricity $r =$ 15°, 30°, 45°, 60°, and 75°. Note that $0 \le \phi \le 30°$ represents a "typical" range of human eye movements, whereas $0 \le \phi \le 60°$ extends to the maximum physical range. The upper limit can be reached, by humans, in the downward direction. The first row of the table gives the mean absolute torsion $|\delta|_0^r$, which was evaluated in the Helmholtz system. These values, which do not seem to have previously been computed, are useful for gauging the significance of the approximation errors. The

TABLE I
ABSOLUTE VALUES OF THE ACTUAL TORSION $\delta(\theta,\phi)$ AND APPROXIMATION ERROR $\epsilon_k(\theta,\phi)$ AVERAGED OVER INCREASINGLY LARGE REGIONS OF THE VIEWING SPHERE

	$r = 15°$	$r = 30°$	$r = 45°$	$r = 60°$	$r = 75°$
$\lvert\delta\rvert_0^r$	$0.314°$	$1.280°$	$2.978°$	$5.596°$	$9.630°$
$\lvert\epsilon_2\rvert_0^r$	$0.001°$	$\mathbf{0.020°}$	$\mathbf{0.112°}$	$\mathbf{0.407°}$	$1.271°$
$\lvert\epsilon_4\rvert_0^r$	$1.45° \times 10^{-5}$	$0.001°$	$0.011°$	$0.075°$	$0.396°$

second and third rows of the table give the average errors ϵ_2 and ϵ_4 that are associated with torsion approximations γ_2 and γ_4, respectively [see (25) and (26)]. Hence, the relative error of the approximations can be computed from $|\epsilon_k|_0^r/|\delta|_0^r$.

The principal conclusion is that the second-order approximation $\gamma_2(\alpha,\beta) = \alpha\beta/2$ has an average error of $0.02°$ for $\phi \leq 30°$ and of $0.4°$ for $\phi \leq 60°$. As fractions of the average torsion $|\delta|_0^r$, these numbers represent errors of 1.6% and 7.3%, respectively. Hence, for typical eye movements ($\phi \leq 30°$), the second-order approximation is adequate, given that eye movements can typically be measured to a precision of around $1°$ [5]. The table also shows that, for all achievable eye movements ($\phi \leq 60°$), the fourth-order model γ_4 is adequate.

IX. SYNTHETIC TORSION

It will now be shown that the results in Sections IV–VII can be used to *synthesize* the effect of Listing's law on images that have been obtained from a pan−tilt camera mounting. Moreover, this operation will be performed in a way that is physically consistent with the original camera, which means that the synthetic image will match the one that would have been obtained after the corresponding cyclorotation of the camera. It is important to ensure physical consistency so that subsequent algorithms need not distinguish between the original and the synthetic images. This requirement cannot, in general, be satisfied by simply rotating the original images around their centerpoints. The appropriate image transformation must be defined in relation to the projection matrix of the camera, as shown in the following discussion. Note that it is usually more convenient and faster to extract features (e.g., points and edges) in the *original* image and then to transform the coordinates of the features. This approach avoids the need to resample or crop the pixel data.

It will be assumed that the camera and ocular projections can be approximated by the usual pin-hole model [1]. Furthermore, it will be assumed that the nodal points of the optics coincide at the fixed rotational center $\boldsymbol{e} = (0,0,0)^\top$ of the camera, as expressed in (2). Each scene point $\boldsymbol{q}$ has coordinates $(x,y,z)^\top$, as described in Section II. The perspective projection is obtained through the 3×3 matrix $\boldsymbol{M}$, which results in homogeneous "eye coordinates" $\boldsymbol{q}_E = (x_E, y_E, z_E)^\top$, with corresponding pixel positions $(x_E/z_E, y_E/z_E)^\top$. This projection means, with reference to (2), that

$$\boldsymbol{q}_E = \boldsymbol{M}\boldsymbol{q} \tag{33}$$

$$= \boldsymbol{S}\boldsymbol{R}^\top\boldsymbol{q} \tag{34}$$

where $\boldsymbol{R}^\top$ is the scene-to-eye rotation, and $\boldsymbol{S}$ performs affine transformation of the image to account for the "intrinsic" parameters of the camera (as described in the following discussion). Note that the rotation is transposed for consistency with (2). In particular, it follows from (1) and (2) that the projection of the fixated point $\boldsymbol{p}$ is $\boldsymbol{S}\boldsymbol{z}$. For a perfect pan−tilt mounting, the rotation $\boldsymbol{R}^\top$ would have the form $\boldsymbol{B}^\top\boldsymbol{A}^\top$ based on (11) and (12). In practice, the camera matrix $\boldsymbol{M}$ [as expressed in (33)] can be estimated by standard methods and decomposed as follows [1]. The matrices $\boldsymbol{S}$ and $\boldsymbol{R}^\top$ [as expressed in (34)] are obtained by RQ-factorization[4] of $\boldsymbol{M}$. The first factor can be written as

$$\boldsymbol{S} = \begin{pmatrix} s_{11} & s_{12} & x_0 \\ 0 & s_{22} & y_0 \\ 0 & 0 & 1 \end{pmatrix}. \tag{35}$$

This matrix contains the pixel coordinates $(x_0, y_0)^\top$ of the principal point (intersection of the optical axis with the image plane), two scale factors (s_{11}, s_{22}), and a parameter $s_{12} \approx 0$ that allows for a skew between the horizontal and vertical axes of the sensor. In more detail, $s_{11} = fg_x$, and $s_{22} = fg_y$, where f is the focal distance of the camera, and the scales (g_x, g_y) determine the number of pixels per unit distance in the horizontal and vertical dimensions.

These intrinsic parameters [see (35)] should not be changed by a synthetic cyclorotation $\boldsymbol{C}^\top$ of the image. Note, however, that the naive procedure $\boldsymbol{C}^\top\boldsymbol{q}_E$ would imply a camera $\boldsymbol{C}^\top\boldsymbol{S}\boldsymbol{R}^\top$ according to the projection model [see (34)]. The matrices $\boldsymbol{C}^\top$ and $\boldsymbol{S}$ do not, in general, commute. It follows that $\boldsymbol{S}$ would not be recovered from the RQ-factorization of the implied camera (due to the uniqueness of the factorization). For this reason, the cyclorotated points are properly defined as

$$\boldsymbol{q}'_E = \boldsymbol{S}\boldsymbol{C}^\top\boldsymbol{S}^{-1}\boldsymbol{q}_E. \tag{36}$$

This definition, with reference to (34), implies the existence of a synthetic camera matrix $\boldsymbol{M}'$. We have

$$\boldsymbol{M}' = \boldsymbol{S}\boldsymbol{C}^\top\boldsymbol{S}^{-1}\boldsymbol{M}$$

$$= \boldsymbol{S}\boldsymbol{C}^\top\boldsymbol{R}^\top.$$

It is clear from (34) that the matrix $\boldsymbol{M}'$ has the RQ-factorization $\boldsymbol{S}\cdot\boldsymbol{C}^\top\boldsymbol{B}^\top\boldsymbol{A}^\top$ and is therefore consistent with the original set of intrinsic parameters [see (35)]. In practice, it may be more convenient to work with "normalized coordinates" $\boldsymbol{S}^{-1}\boldsymbol{q}_E$, where the effects of the intrinsic parameters have been undone. In this case, the cyclorotated and normalized coordinates are simply

$$\boldsymbol{q}''_E = \boldsymbol{C}^\top\boldsymbol{S}^{-1}\boldsymbol{q}_E. \tag{37}$$

The product $\boldsymbol{C}^\top\boldsymbol{S}^{-1}$ can first be formed so that a single affine transformation is applied to the observed feature coordinates $\boldsymbol{q}_E$. Note that this mapping is a 2-D transformation, depending

[4]The decomposition $M = RQ$ has an upper triangular factor R and an orthogonal factor Q. The decomposition is unique if, as is the case in this paper, M has full rank and R is required to have positive elements on the diagonal.

only on the intrinsic parameters (35) and the cyclorotation angle γ. In the special case that the upper left 2×2 block of $\boldsymbol{S}$ is a multiple $s\boldsymbol{I}_2$ of the identity matrix, the procedure (37) simply translates the principal point $(x_0, y_0)^\top$ to $(0, 0)^\top$ before scaling and rotating the feature coordinates by s and γ, respectively. In general, however, $s_{11} \neq s_{22}$, and $s_{12} \neq 0$, which mean that the transformation (37) should be used.

If the cyclorotation angle γ is defined by (22), then the new coordinates $\boldsymbol{q}''_E$ (and the Q factor of the implied camera matrix) are subject to Listing's law and are physically consistent with the original camera. Other aspects of biological vision, e.g., the nonuniform distribution of photoreceptors on the retina [35], can be modeled by further transformations of the new coordinates. It is also possible to adapt the aforementioned model to a spherical projection, which may be more appropriate for the human eye; in this case, the observed feature coordinates are $(x_E/d, y_E/d)^\top$, where $d = |\boldsymbol{q}|$ is the distance to the point, as expressed in (1).

X. Discussion

It has been shown in Sections II–VI that Listing's law can be formulated in terms of rotation matrices. This means that the usual computer vision camera-model (34) can easily be adapted to the human eye, as shown in Section IX. Two polynomial approximations of the torsion function $\gamma(\alpha, \beta)$ were derived in Section VII. A procedure for numerical integration over visual directions was introduced in Section VIII. The average cyclo-rotation was computed, and the two approximations were validated. Finally, in Section IX, it was shown that Listing's law can be imposed on a suitable set of calibrated images.

There is considerable interest in the relationship between Listing's law and other visual processes, such as spatial vision and stereopsis [2], [4], and [38]. For example; if the binocular fixation point is relatively close, then Listing's law must be modified [36], [37]. Future work will include an extension of the present analysis to the binocular case [15]. The results presented here, as described in the introduction, make it possible to evaluate such models with respect to real images.

The implications of Section VII, with regard to the neural representation of eye-movements, are also interesting. It is clear that the cyclo-rotation angle is a slowly-varying function of visual direction, over the typical range of eye movements. Indeed, the results of Section VIII show that the observed cyclo-rotation is effectively proportional the product of the eye's azimuth and elevation. This suggests that Listing's law could be be represented quite directly in the primate oculomotor system [3].

References

[1] R. Hartley and A. Zisserman, *Multiple-View Geometry in Computer Vision*. Cambridge, U.K.: Cambridge Univ. Press, 2000.

[2] J. J. Koenderink and A. van Doorn, "Geometry of binocular vision and a model for stereopsis," *Biol. Cybern.*, vol. 21, no. 1, pp. 29–35, Jan. 1976.

[3] A. V. van den Berg, "Kinematics of eye movement control," *Proc. R. Soc. Lond. B*, vol. 260, no. 1358, pp. 191–197, May 1995.

[4] D. Tweed, "Visual-motor optimization in binocular control," *Vis. Res.*, vol. 37, no. 14, pp. 1939–1951, Jul. 1997.

[5] R. H. S. Carpenter, *Movements of the Eyes*. London, U.K.: Pion, 1988.

[6] H. L.F. von Helmholtz, *Treatise on Physiological Optics*, 3rd ed., vol. III. New York: Opt. Soc. Amer., 1925. trans. J. P. C. Southall.

[7] D. Tweed and T. Vilis, "Geometric relations of eye position and velocity vectors during saccades," *Vis. Res.*, vol. 30, no. 1, pp. 111–127, 1990.

[8] D. Tweed, W. Cadera, and T. Vilis, "Computing three-dimensional eye position quaternions and eye velocity from search coil signals," *Vis. Res.*, vol. 30, no. 1, pp. 97–110, 1990.

[9] P. S. Sandor, M. A. Frens, and V. Henn, "Chameleon eye position obeys Listing's law," *Vis. Res.*, vol. 41, no. 17, pp. 2245–2251, Aug. 2001.

[10] W. Zhu and W. M. King, "Binocular eye movements not coordinated during REM sleep," *Exp. Brain Res.*, vol. 117, no. 1, pp. 153–160, Oct. 1997.

[11] K. Hepp, "Theoretical explanations of Listing's law and their implications for binocular vision," *Vis. Res.*, vol. 35, no. 23/24, pp. 3237–3241, Dec. 1995.

[12] G. Westheimer, "Kinematics of the eye," *J. Opt. Soc. Amer.*, vol. 47, no. 10, pp. 967–974, 1957.

[13] D. A. Robinson, "A quantitative analysis of extraocular muscle cooperation and squint," *Invest. Ophthalmol.*, vol. 14, no. 11, pp. 801–825, Nov. 1975.

[14] T. Haslwanter, "Mathematics of three-dimensional eye rotations," *Vis. Res.*, vol. 35, no. 12, pp. 1727–1739, Jun. 1995.

[15] M. Hansard and R. Horaud, "Cyclopean geometry of binocular vision," *J. Opt. Soc. Amer. A, Opt. Image Sci.*, vol. 25, no. 9, pp. 2357–2369, Sep. 2008.

[16] O. Bolina and L. H. A. Monteiro, "Kinematics of eye movement," *Ophthalmic Physiol. Opt.*, vol. 20, no. 1, pp. 59–62, Jan. 2000.

[17] D. W. Murray, F. Du, P. F. McLauchlan, I. D. Reid, P. M. Sharkey, and M. Brady, "Design of stereo heads," in *Active Vision*, A. Blake and A. Yuille, Eds. Cambridge, MA: MIT Press, 1992.

[18] J. P. Barreto and H. Araujo, "General framework for selecting world coordinate systems in perspective and catadioptric imaging applications," *Int. J. Comput. Vis.*, vol. 57, no. 1, pp. 23–47, Apr. 2004.

[19] M. R. M. Jenkin and J. K. Tsotsos, "Active stereo vision and cyclotorsion," in *Proc. IEEE CVPR*, 1994, pp. 806–811.

[20] G. Cannata and M. Maggiali, "Models for the design of bioinspired robot eyes," *IEEE Trans. Robot.*, vol. 24, no. 1, pp. 27–44, Feb. 2008.

[21] D. A. Robinson, "The oculomotor control system: A review," *Proc. IEEE*, vol. 56, no. 6, pp. 1032–1049, Jun. 1968.

[22] L. R. Young and D. Sheena, "Survey of eye movement recording methods," *Behav. Res. Methods Instrum.*, vol. 7, no. 5, pp. 397–439, 1975.

[23] K. R. Park, "A real-time gaze position estimation method based on a 3-D eye model," *IEEE Trans. Syst., Man, Cybern. B: Cybern.*, vol. 37, no. 1, pp. 199–212, Feb. 2007.

[24] A. Villanueva and R. Cabeza, "A novel gaze estimation system with one calibration point," *IEEE Trans. Syst., Man, Cybern. B: Cybern.*, vol. 38, no. 4, pp. 1123–1138, Aug. 2008.

[25] T. Haslwanter and S. T. Moore, "A theoretical analysis of three-dimensional eye position measurement using polar cross correlation," *IEEE Trans. Biomed. Eng.*, vol. 42, no. 11, pp. 1053–1061, Nov. 1995.

[26] J. Stuelpnagel, "On the parametrization of the three-dimensional rotation group," *SIAM Rev.*, vol. 6, no. 4, pp. 422–430, Oct. 1964.

[27] W. Haustein, "Considerations on Listing's law and the primary position by means of a matrix description of eye position control," *Biol. Cybern.*, vol. 60, no. 6, pp. 411–420, Apr. 1989.

[28] K. Hepp, "On Listing's law," *Commun. Math. Phys.*, vol. 132, no. 1, pp. 285–292, Aug. 1990.

[29] D. Hestenes, "Invariant body kinematics I: Saccadic and compensatory eye movements," *Neural Netw.*, vol. 7, no. 1, pp. 65–77, 1994.

[30] S. Judge, "Reflection makes sense of rotation of the eyes," *Vis. Res.*, vol. 46, no. 22, pp. 3862–3866, Oct. 2006.

[31] R. A. B. Somani, J. F. X. Desouza, D. Tweed, and T. Vilis, "Visual test of Listing's law during vergence," *Vis. Res.*, vol. 38, no. 6, pp. 911–923, Mar. 1998.

[32] I. T. C. Hooge and A. V. van den Berg, "Visually evoked cyclovergence and extended Listing's law," *J. Neurophysiol.*, vol. 83, no. 5, pp. 2757–2775, May 2000.

[33] A. T. Bahill, D. Adler, and L. Stark, "Most naturally occurring human saccades have magnitude of 15 degrees or less," *Invest. Ophthalmol.*, vol. 14, no. 6, pp. 468–469, Jun. 1975.

[34] A. Genz and A. A. Malik, "An adaptive algorithm for numerical integration over an N-dimensional rectangular region," *J. Comput. Appl. Math.*, vol. 6, pp. 295–302, 1980.

[35] C. A. Curcio, K. R. Sloan, R. E. Kalina, and A. E. Hendrickson, "Human photoreceptor topography," *J. Comp. Neurol.*, vol. 292, no. 4, pp. 497–523, Feb. 1990.

[36] D. Mok, A. Ro, W. Cadera, J. D. Crawford, and T. Vilis, "Rotation of Listing's plane during vergence," *Vis. Res.*, vol. 32, no. 11, pp. 2055–2064, Nov. 1992.

[37] L. J. van Rijn and A. V. van den Berg, "Binocular eye orientation during fixation: Listing's law extended to include eye vergence," *Vis. Res.*, vol. 33, no. 5/6, pp. 691–708, Mar./Apr. 1993.
[38] K. Nakayama and R. Balliet, "Listing's Law, eye position sense, and perception of the vertical," *Vis. Res.*, vol. 17, no. 3, pp. 453–457, 1977.

Miles Hansard received the B.Sc. degree in experimental psychology, the M.Res. degree, and the Ph.D. degree in computer vision from University College London, London, U.K.

He is currently a Postdoctoral Researcher with the Institut National de Recherche en Informatique et en Automatique, Rhône-Alpes, Montbonnot, France. His research interests include geometric and computational aspects of visual perception. His recent research work has been focused on human and robotic stereopsis.

Radu Horaud received the B.Sc. degree in electrical engineering, the M.Sc. degree in control engineering, and the Ph.D. degree in computer science from the Institut National Polytechnique de Grenoble, Grenoble, France.

He holds a position of Director of Research with the Institut National de Recherche en Informatique et en Automatique, Rhône-Alpes, Montbonnot, France. His research interests include computer vision, machine learning, multisensory fusion, and robotics. He is the author of more than 100 scientific publications. He is an Area Editor of *Elsevier Computer Vision and Image Understanding*, a member of the advisory board of the *Sage International Journal of Robotics Research*, and a member of the editorial boards of the *Kluwer International Journal of Computer Vision*, *Image and Vision Computing*, and *Springer Machine Vision and Applications*.

Dr. Horaud was a Program Cochair of the Eighth IEEE International Conference on Computer Vision (ICCV 2001).